

Structure and magnetic order in undoped lanthanum manganite

Q. Huang

*Reactor Radiation Division, National Institute of Standards and Technology, Gaithersburg, Maryland 20899
and Materials Research Program, University of Maryland, College Park, Maryland 20742*

A. Santoro

Reactor Radiation Division, National Institute of Standards and Technology, Gaithersburg, Maryland 20899

J. W. Lynn

*Reactor Radiation Division, National Institute of Standards and Technology, Gaithersburg, Maryland 20899
and Center for Superconductivity Research, University of Maryland, College Park, Maryland 20742*

R. W. Erwin and J. A. Borchers

Reactor Radiation Division, National Institute of Standards and Technology, Gaithersburg, Maryland 20899

J. L. Peng and R. L. Greene

Center for Superconductivity Research, University of Maryland, College Park, Maryland 20742

(Received 22 July 1996; revised manuscript received 16 October 1996)

The undoped lanthanum manganite system of nominal composition LaMnO_3 has been analyzed by neutron powder diffraction for different sample heat treatment methods. Four distinct crystallographic phases have been identified: (i) an orthorhombic phase of space group $Pnma$ and lattice parameters (at 300 K) $a = 5.7385(3)$, $b = 7.7024(3)$, $c = 5.5378(2)$ Å, produced by annealing in a reducing atmosphere. The system develops long-range antiferromagnetic order below $T_N = 140$ K with the Mn^{3+} spins coupled ferromagnetically in the a - c plane and antiferromagnetically along b , with the spin direction along a . The volume of this phase increases monotonically with increasing temperature, but both the a and c lattice parameters exhibit negative thermal expansion in alternate temperature regimes. (ii) A second (previously unreported) orthorhombic phase that exhibits a smaller splitting, also of space group $Pnma$ and lattice parameters (at 300 K) $a = 5.4954(3)$, $b = 7.7854(4)$, $c = 5.5355(3)$ Å, produced by annealing in an oxygen (or air) atmosphere. This system orders with a simple ferromagnetic structure at $T_c = 140$ K, with the spin direction along c . Phases (i) and (ii) can be transformed reversibly by suitable heat treatment of the same sample, and exist with a range of lattice parameters and compositions. The unit-cell volume for the antiferromagnetic phase is considerably larger than for the ferromagnetic phase, which agrees with the double-exchange model proposed for this system. (iii) A monoclinic phase of space group $P112_1/a$ and lattice parameters (at 200 K) $a = 5.4660(4)$, $b = 7.7616(7)$, $c = 5.5241(5)$ Å, $\gamma = 90.909^\circ(5)$ that orders ferromagnetically below 140 K. (iv) A rhombohedral phase of space group $R\bar{3}c$ and hexagonal lattice parameters (at 300 K) $a = 5.5259(2)$, $c = 13.3240(4)$ Å, that is observed only above room temperature. Occupancy refinements show that phase (i) ideally has the stoichiometric composition LaMnO_3 , while the results for the Mn-O bond distances suggest that phases (ii), (iii), and (iv) are progressively richer in oxygen (and thus Mn^{4+}). The results of our study strongly suggest the progressive development of cation vacancies in equal numbers on the La and Mn sites as the oxygen content is increased by heat treatment. In the monoclinic phase the Mn ions occupy two crystallographically independent sites, but no evidence of ordering of Mn^{3+} and Mn^{4+} was observed. The structures of the four phases are closely related to that of perovskite. The MnO_6 octahedra are tilted from the undistorted configuration, the tilt system being $a^- a^- a^-$ in the rhombohedral structure and $a^+ b^- b^-$ in both orthorhombic modifications.

[S0163-1829(97)04122-2]

I. INTRODUCTION

Lanthanum manganite (nominal composition LaMnO_3) is an insulating material that orders magnetically at around 150 K. Doping with cations such as Ca, Ba, or Sr induces a metal-insulator transition that is associated with the magnetic order, and the recent discovery of huge magnetoresistance effects associated with these phase transitions has rekindled intense interest in this class of materials.¹ To achieve an overall understanding of the behavior of the doped systems it

is desirable to have a thorough understanding of the undoped parent LaMnO_3 compound as a starting basis. The reported properties for LaMnO_3 , however, have varied rather dramatically both in terms of the crystal structure observed, and whether it is an antiferromagnet or a ferromagnet.

The magnetic and structural properties of $\text{La}_{1-x}\text{Ca}_x\text{MnO}_3$ ($0 \leq x \leq 1$) were first characterized by Wolan and Koehler² and by Yakel³ for several compositions x . Room-temperature x-ray powder diffraction patterns of samples of the undoped compound ($x=0$) showed mono-

TABLE I. Sample preparation conditions and phase relations.

Symbol	Preparation condition	T (K)	Nuclear structure					Magnetic property		
			Space group	a (Å)	b (Å)	c (Å)	γ (°)	State	$\mu_{\text{Mn}}(\mu_B)$	T_C, T_N (K)
LaMnO ₃ -I	1350 °C (2 days) in air	10	$P112_1/a$ (15 wt %)	5.4623(7)	7.751(1)	5.5225(7)	90.97°	FM	1.54(4)	~131
			$Pnma$ (85 wt %)	5.4780(2)	7.7587(2)	5.5218(2)		FM	1.54(4)	~131
		300	$R\bar{3}c$ (71 wt %)	5.5259(2)		13.3240(4)				
LaMnO ₃ -II	Sample I, 1450 °C (1 h), annealed in N ₂ at 900 °C (2 h) with Ti metal next to sample	10	$Pnma$ -1(20 wt %)	5.5345(8)	7.719(1)	5.6094(6)		FM	2.7(2)	
			$Pnma$ -2(80 wt %)	5.6685(2)	7.6882(3)	5.5325(3)		AFM	3.42(3)	
		300	$Pnma$ -1(20 wt %)	5.5387(8)	7.746(1)	5.6093(6)				
			$Pnma$ -2(80 wt %)	5.6688(2)	7.7238(3)	5.5355(3)				
LaMnO ₃ -IIa	Sample II, annealed in N ₂ at 900 °C (5 h) with Ti metal next to sample	14	$Pnma$	5.7400(1)	7.6738(2)	5.5328(1)		AFM	3.64(3)	~138
		300	$Pnma$	5.7385(3)	7.7024(3)	5.5378(2)				
LaMnO ₃ -IIb	Sample II, annealed in air at 1000 °C (12 h)	15	$Pnma$	5.4913(2)	7.7748(3)	5.5268(2)		FM	2.94(4)	~140
		300	$R\bar{3}c$ (12 wt %)	5.5316(6)		13.330(1)				
			$Pnma$ (88 wt %)	5.4954(3)	7.7854(4)	5.5355(3)				
LaMnO ₃ -III	1350 °C (2 days) in air	10	$Pnma$	5.4947(2)	7.7745(3)	5.5251(2)		FM	2.67(5)	~123
		300	$Pnma$	5.4975(2)	7.7867(3)	5.5341(2)				
LaMnO ₃ -IV	1350 °C (2 days) and 1450 °C (1 h) in air, annealed in argon at 1000 °C (10 h)	10	$Pnma$ -1(22 wt %)	5.526(1)	7.742(1)	5.6081(8)		FM	2.8(2)	
			$Pnma$ -2(78 wt %)	5.6692(2)	7.6850(4)	5.5322(3)		AFM	3.39(4)	
		300	$Pnma$ -1(24 wt %)	5.5316(9)	7.755(1)	5.6037(8)				
			$Pnma$ -2(76 wt %)	5.6590(2)	7.7194(3)	5.5344(3)				

clinic or orthorhombic symmetry in some cases, and rhombohedral symmetry in others, with slight or no splitting of the diffraction peaks at low temperatures. Such variations of structure were observed in materials obtained with different methods of preparation, and were always accompanied by more or less pronounced departures from the stoichiometric composition.³ Below $T_N \approx 140$ K, the magnetic moments of the Mn³⁺ ions of samples with 2% or less Mn⁴⁺, were found to be ordered ferromagnetically along two axes of the original perovskite cell, and antiferromagnetically along the third direction, resulting in a structure (labeled *A-8-0* by Wollan and Koehler) in which each Mn³⁺ ion is coupled ferromagnetically to four of its neighbors and antiferromagnetically to the other two. This arrangement of the magnetic moments was found to be consistent with the theoretical predictions derived by Goodenough for the Mn-O bonding and the

Mn-Mn magnetic exchange in the system [La,*M*(II)]MnO₃.⁴ Samples containing 10% or more Mn⁴⁺ gave powder patterns consistent with an incoherent mixture of regions or domains having antiferro- and ferromagnetic ordering (referred as structural types *A-8-0* and *B-6-2*, respectively, in Ref. 2).

The crystallographic and magnetic structures of stoichiometric LaMnO₃ were analyzed more recently by Elemans *et al.* by x-ray and neutron powder diffraction methods.⁵ These authors found the compound to be orthorhombic, space group $Pnma$. A fairly precise determination of the oxygen positions allowed them to establish that the MnO₆ octahedra are not only distorted, but also rotated from the ideal perovskite orientation. The magnetic structure reported in this study is antiferromagnetic of the type determined in Ref. 2 and has magnetic space group symmetry $Pn'ma'$,

TABLE II. Occupancy refinements. Data collected at 300 K. Space group: $Pnma$. The occupancies of O sites were fixed at 1.

Sample and magnetic ordering state	Occupancy		B (Å ²) for				R_p (%)	R_{wp} (%)	χ^2
	La	Mn	La	Mn	O(1)	O(2)			
LaMnO ₃ -IIa AFM	1	1	0.62(3)	0.61(5)	0.79(4)	0.79(3)	5.92	7.49	1.326
	1.007(9)	1.01(2)	0.63(4)	0.63(8)	0.77(5)	0.77(3)	5.91	7.46	1.326
LaMnO ₃ -IIb FM	1	1	0.98(4)	0.69(6)	1.20(6)	1.14(4)	6.30	7.86	1.222
	0.953(6)	0.95(2)	0.89(5)	0.55(8)	1.28(6)	1.27(5)	6.21	7.79	1.200
LaMnO ₃ -III FM	1	1	0.92(2)	0.66(3)	1.22(4)	1.05(3)	5.48	6.91	1.466
	0.988(5)	0.979(7)	0.92	0.66	1.22	1.05	5.45	6.89	1.454
	0.972(8)	0.94(1)	0.88(3)	0.45(6)	1.29(4)	1.15(7)	5.37	6.84	1.437
	0.95	0.95	0.81(2)	0.54(3)	1.30(4)	1.18(3)	5.40	6.85	1.439

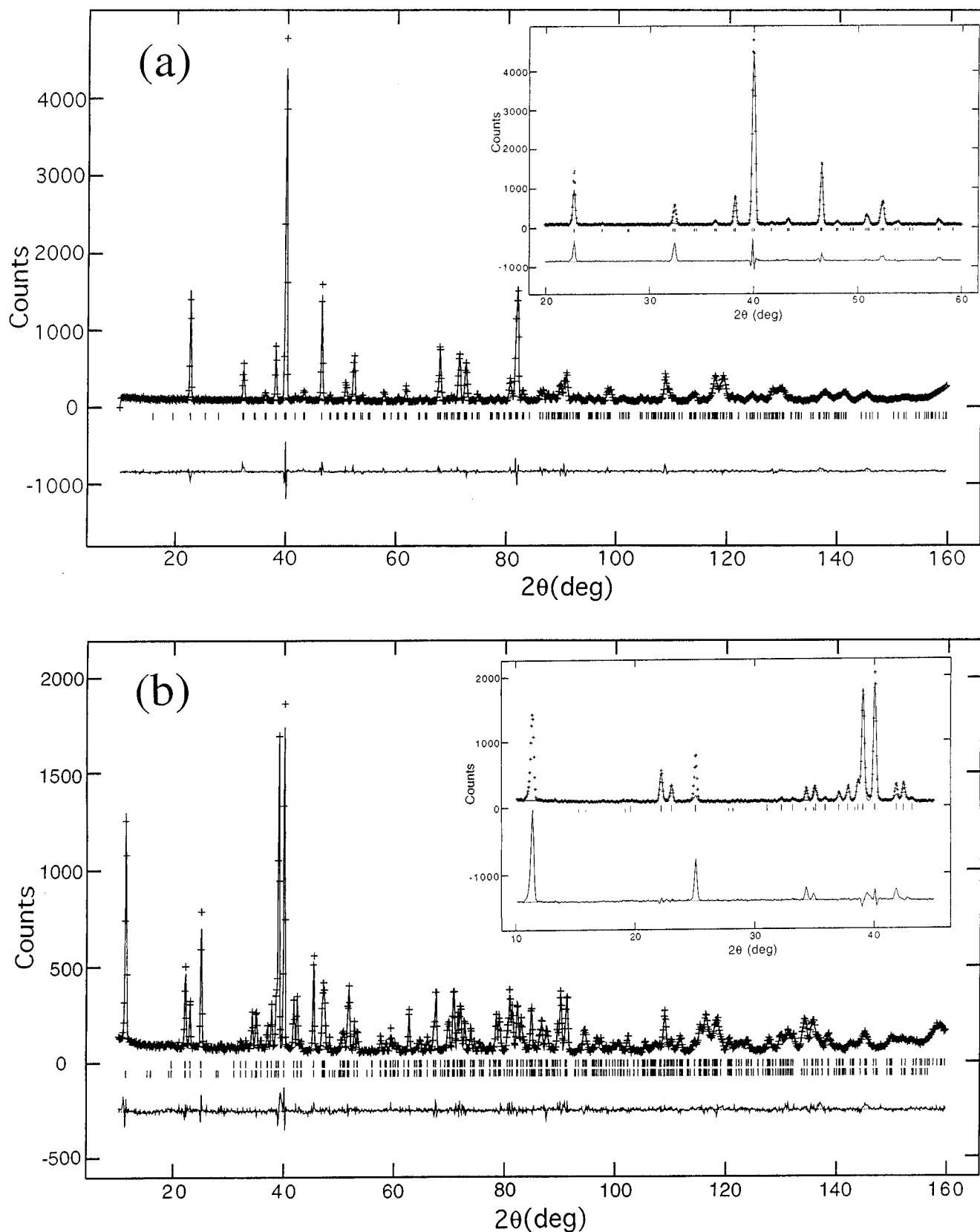


FIG. 1. (a) Plot of observed and calculated intensity profiles for sample IIb at 10 K (pure phase *Pnma*, ferromagnetic); (b) same plot for sample IIa (pure phase *Pnma*, antiferromagnetic). In both patterns, the short vertical lines indicate the angular positions of nuclear (top row) and magnetic (bottom row) Bragg reflections. The lower parts of both figures show the difference plot $I(\text{obs})-I(\text{calc})$. The plots in the inset show the observed intensities and those calculated for the nuclear structure only, so that the magnetic contribution is visible in the difference plot at the bottom in each inset.

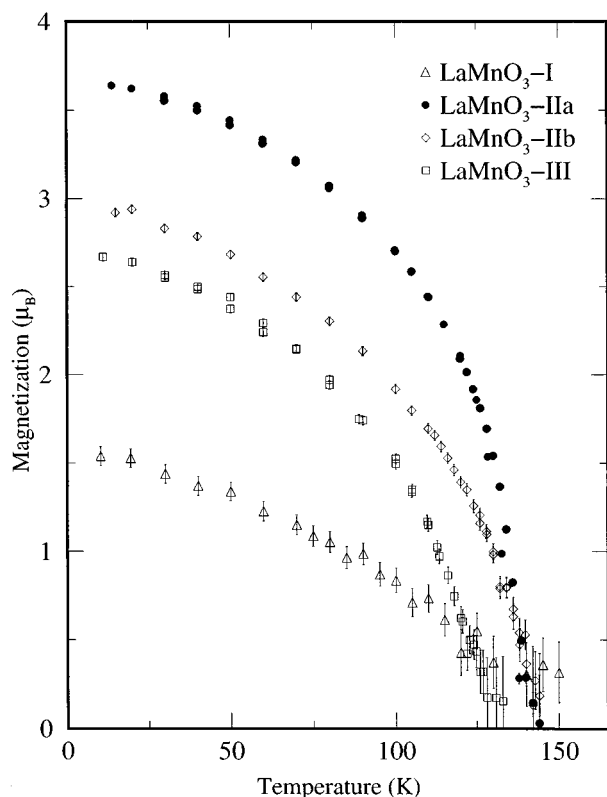


FIG. 2. Temperature dependence of the magnetization (open symbols) or sublattice magnetization (solid symbols) for the various samples.

with the moments aligned along the a axis of the unit cell.

A different nuclear structure was subsequently found for the compound of composition $\text{LaMnO}_{3.12}$.⁶ A room-temperature neutron-diffraction analysis showed that this material crystallizes with the symmetry of space group $R\bar{3}c$ and has a structure in which the MnO_6 octahedra are distorted and tilted about one of the $\langle 111 \rangle$ threefold axes of the original perovskite cell. Refinements of various structural models gave the best agreement between observed and calculated intensities for a composition corresponding to the formula $(\text{La}_{0.94(2)}\square_{0.06(2)})(\text{Mn}_{0.745}^{3+}\text{Mn}_{0.235}^{4+}\square_{0.02})\text{O}_3$, with partial elimination of La_2O_3 and the presence of vacancies \square on both the A and B metal sites. Unfortunately, no determination of the magnetic structure is reported in this paper. Cation vacancies rather than defects at the oxygen sites were also found in subsequent studies,^{7,8} but in these cases the best agreement between observed and calculated intensities was obtained when the occupancies of La and Mn were constrained to be equal.

Magnetic and resistivity measurements recently carried out for a broad range of compositions in $\text{La}_{1-x}\text{Ca}_x\text{MnO}_3$ show a low-temperature insulator to metal transition at $x \approx 0.18$,⁹ with ferromagnetic ordering for $x < 0.5$. In particular, ferromagnetic order was found for the undoped $x = 0$ material, in agreement with the results on our initial $x = 0$ sample.¹⁰ These observations are at variance with the results obtained in some previous investigations,^{2,5} and we have therefore undertaken a detailed investigation of the undoped material in order to clarify the parameters controlling the

chemical and magnetic structures of this material. We have found that stoichiometric LaMnO_3 is an antiferromagnet with an orthorhombic crystal structure. Annealing in oxygen, on the other hand, introduces small amounts of additional oxygen in the system, where this additional oxygen appears to be accommodated by introducing La and Mn vacancies in the structure. This has the effect of changing the magnetic structure from antiferromagnetic to ferromagnetic, while crystallographically the orthorhombic splitting is first reduced in size as the number of defects increases, and then a monoclinic-rhombohedral structure is formed.

II. EXPERIMENTAL DETAILS

All samples used in this study were prepared by mixing the appropriate quantities of La_2O_3 and MnCO_3 and heating the mixture in air at about 1350°C for 2 days, with several intermediate grindings. After this treatment, one of the samples (sample II in Table I) was heated to 1450°C for 1 h, before the furnace was allowed to cool to room temperature. Annealing conditions, where applicable, are indicated in Table I. In order to check if the gas atmosphere has any influence on the products of the reaction, the reducing heat treatments, originally carried out in an atmosphere of nitrogen, were repeated in argon under the same conditions, with the same results.

The neutron powder diffraction measurements were made with the BT-1 high-resolution powder diffractometer at the reactor of the National Institute of Standards and Technology (NIST) using neutron beams of wavelength $1.5396(1)$ and $1.5899(1)$ Å produced by a copper (311) and a silicon (531) monochromator, respectively. Collimators with horizontal divergences of $15'$, $20'$, and $7'$ full width at half maximum were used for the in-pile, monochromatic and diffracted beams, respectively. The intensities were measured in steps of 0.05° in the 2θ range 3° – 165° . The scattering amplitudes used in all calculations are $b(\text{La}) = 0.827$, $b(\text{Mn}) = 0.344$, and $b(\text{O}) = 0.581$ ($\times 10^{-12}$ cm). Crystal structure refinements were carried out using the program GSAS of Larson and Von Dreele,¹¹ and adopting as initial models slightly distorted structures derived from the original perovskite configuration. Data were typically collected at a series of temperatures in order to elucidate both the nuclear and magnetic structures and to detect possible phase transitions. The intensity of one of the strong magnetic Bragg peaks was monitored as a function of temperature with the BT-2 or BT-9 triple-axis spectrometer, using a pyrolytic graphite monochromator and filter, which provided much higher intensity than BT-1. The phase composition of each sample, the space group, lattice parameters, and the nature of the magnetic ordering, are summarized in Table I.

III. RESULTS

As mentioned in the Introduction, the formation of cation vacancies on both the La and Mn sites has been reported in the literature when the samples are oxidized.^{6–8} In order to check this structural aspect for our compounds, refinements of cation occupancies were carried out for samples IIa, IIb, and III, and the results of these calculations are listed in Table II. In some of these refinements the oxygen occupan-

TABLE III. (Top) Structural parameters of LaMnO_3 -I. The atomic positions for space group $R\bar{3}c$ (No. 167): La: $6a(0,0,1/4)$, Mn: $6b(0,0,0)$, and O: $18e(x,0,1/4)$; for $Pnma$ (No. 62): La: $4c(x,1/4,z)$, Mn: $4b(0,0,1/2)$, O(1) $4c(x,1/4,z)$, and O(2): $8d(x,y,z)$; for $P112_1/a$ (No. 14): La: $4e(x,y,z)$, Mn(1): $2c(1/2,0,0)$, Mn(2): $2d(1/2,1/2,0)$, O(1): $4e(x,y,z)$, O(2): $4e(x,y,z)$, and O(3): $4e(x,y,z)$. The magnetic structural models have $P1$ symmetry with Mn moments parallel to the a or b axis for the $R\bar{3}c$ phase, and $Pn'm'a$ and $P112_1/a$ symmetry with Mn moments parallel to the c axis for the $Pnma$ and $P112_1/a$ phases, respectively. The temperature parameters B of La, Mn, and O(1), and the magnetic moments of Mn are constrained to be the same in the $Pnma$ and $P112_1/a$ refinements. $B[\text{O}(2)]$ in $Pnma$ is constrained to be equal to $B[\text{O}(2)]$ and $B[\text{O}(3)]$ in $P112_1/a$. (Bottom) Selected bond distances (\AA) and angles ($^\circ$) of LaMnO_3 -I.

T (K)	10	120	300	350	450
		$P112_1/a$		$R\bar{3}c$	
a (\AA)	5.4623(7)	5.4645(6)	5.4697(7)	5.5285(2)	5.5316(1)
b (\AA)	7.751(1)	7.753(1)	7.773(1)		
c (\AA)	5.5225(7)	5.5244(7)	5.5255(4)	13.3348(4)	13.3539(3)
γ ($^\circ$)	90.97(1)	90.926(9)	90.862(6)		
V (\AA^3)	233.79(4)	234.02(4)	234.90(7)	351.97(3)	353.86(2)
Fraction (wt %)	15	16	72	80	90
La x	0.003(2)	0.008(2)	0.004(2)		
y	0.267(1)	0.262(2)	0.255(1)		
z	-0.013(3)	-0.017(2)	0.005(2)		
B (\AA^2)	0.74(2)	0.86(3)	1.07(3)	1.27(3)	1.37(2)
Mn(1) B (\AA^2)	0.48(3)	0.62(3)	0.71(3)	0.8(4)	0.93(3)
μ (μ_B)	1.54(4)				
Mn(2) B (\AA^2)	0.48(3)	0.62(3)	0.71(3)		
μ (μ_B)	1.54(4)				
O(1) x	0.491(5)	0.499(4)	0.491(2)	0.4466(1)	0.4473(2)
y	0.246(2)	0.243(3)	0.253(1)		
z	0.055(3)	0.057(3)	0.059(2)		
B (\AA^2)	0.90(4)	1.01(4)	1.35(9)	1.28(3)	1.54(3)
O(2) x	0.216(4)	0.236(4)	0.227(2)		
y	0.033(2)	0.029(2)	0.030(2)		
z	-0.239(5)	-0.234(5)	-0.234(2)		
B (\AA^2)	0.73(3)	0.99(3)	1.08(6)		
O(3) x	-0.276(4)	-0.284(4)	-0.269(3)		
y	0.537(2)	0.535(2)	0.528(2)		
z	0.257(4)	0.270(5)	0.276(2)		
B (\AA^2)	0.73(3)	0.99(3)	1.08(6)		
		$Pnma$			
a (\AA)	5.4780(2)	5.4794(2)	5.4910(4)	5.4955(6)	5.503(1)
b (\AA)	7.7587(3)	7.7606(3)	7.7764(7)	7.7804(9)	7.788(1)
c (\AA)	5.5218(2)	5.5237(2)	5.5323(4)	5.5358(5)	5.5431(9)
V (\AA^3)	234.69(2)	234.89(2)	236.23(3)	236.69(3)	237.57(5)
Fraction (wt %)	85	84	28	20	10
La x	-0.0204(3)	-0.0196(3)	-0.0198(8)	-0.020(1)	-0.020(3)
z	-0.0032(4)	-0.0027(4)	-0.006(1)	-0.003(2)	-0.009(3)
B (\AA^2)	0.74(2)	0.86(3)	1.07(3)	1.27(3)	1.37(3)
Mn B (\AA^2)	0.48(3)	0.62(3)	0.71(3)	0.80(4)	0.93(3)
μ (μ_B)	1.54(4)				
O(1) x	0.5063(5)	0.5065(5)	0.509(1)	0.509(2)	0.506(6)
z	0.0633(5)	0.0634(5)	0.063(1)	0.064(2)	0.061(4)
B (\AA^2)	0.90(4)	1.01(4)	1.35(9)	1.28(3)	1.54(3)
O(2) x	0.2278(3)	0.2278(3)	0.2288(9)	0.229(1)	0.235(2)
y	0.0333(2)	0.0334(2)	0.0331(5)	0.0343(7)	0.037(1)
z	-0.2293(3)	-0.2292(3)	-0.229(1)	-0.226(1)	-0.229(2)
B (\AA^2)	0.73(3)	0.99(3)	1.08(6)	1.28(3)	1.54(3)
R_p (%)	5.62	5.08	4.53	5.67	4.95
R_{wp} (%)	7.04	6.37	5.84	6.73	6.19
χ^2	1.451	1.312	1.171	1.001	1.101

TABLE III. (Continued).

T (K)	10	120	300	350	450
		$P112_1/a$			$R\bar{3}c$
La-O(1)	2.82(2)	2.81(3)	2.81(1)	3.060(1)×3	3.057(1)×3
La-O(1)	2.71(3)	2.72(3)	2.69(1)		
La-O(1)	3.00(2)	2.99(2)	3.12(2)		
La-O(1)	2.53(3)	2.55(2)	2.41(2)	2.469(1)×3	2.475(1)×3
La-O(2)	2.51(2)	2.52(2)	2.52(1)		
La-O(2)	3.19(2)	3.10(2)	3.05(2)		
La-O(2)	2.95(2)	2.95(2)	2.83(2)	2.7521(1)×6	2.7547(1)×6
La-O(2)	2.74(3)	2.70(3)	2.74(2)		
La-O(3)	3.00(2)	3.10(3)	3.01(2)		
La-O(3)	2.35(2)	2.33(2)	2.48(1)		
La-O(3)	2.51(3)	2.57(3)	2.70(2)		
La-O(3)	2.78(2)	2.75(2)	2.72(2)		
Mn(1)-O(1)×2	1.99(2)	2.02(2)	1.94(1)	1.9671(2)×6	1.9680(6)×6
Mn(1)-O(3)×2	2.04(2)	2.03(3)	1.94(1)		
Mn(1)-O(3)×2	1.89(2)	1.92(3)	1.99(1)		
Mn(2)-O(1)×2	1.93(2)	1.91(2)	2.00(1)		
Mn(2)-O(2)×2	2.06(3)	1.95(3)	1.99(1)		
Mn(2)-O(2)×2	1.87(3)	1.97(3)	1.94(1)		
Mn(1)-O(1)-Mn(2)	161.5(10)	161.6(10)	160.8(6)	162.71(6)	162.98(6)
Mn(2)-O(2)-Mn(2)	161.7(10)	165.0(10)	163.5(7)		
Mn(1)-O(3)-Mn(1)	161.5(10)	160.0(11)	163.5(7)		
			$Pnma$ phase		
La-O(1)	2.619(3)	2.622(3)	2.618(8)	2.61(1)	2.64(3)
La-O(1)	2.909(3)	2.906(3)	2.929(8)	2.93(1)	2.92(3)
La-O(1)	3.096(3)	3.101(3)	3.088(9)	3.11(1)	3.07(3)
La-O(1)	2.433(3)	2.430(3)	2.454(9)	2.44(1)	2.48(3)
La-O(2)×2	2.497(2)	2.496(2)	2.497(6)	2.492(2)	2.49(2)
La-O(2)×2	3.113(2)	3.111(2)	3.121(5)	3.137(9)	3.14(1)
La-O(2)×2	2.788(2)	2.789(2)	2.802(5)	2.975(8)	2.86(1)
La-O(2)×2	2.629(2)	2.634(2)	2.627(7)	2.639(9)	2.58(2)
Mn-O(1)×2	1.9712(5)	1.9723(5)	1.976(1)	1.978(2)	1.977(4)
Mn-O(2)×2	1.973(1)	1.973(1)	1.972(5)	1.962(6)	1.96(1)
Mn-O(2)×2	1.964(2)	1.966(2)	1.973(6)	1.991(7)	2.00(1)
Mn-O(1)-Mn	159.5(2)	159.4(2)	159.5(4)	159.1(6)	160(1)
Mn-O(2)-Mn	162.01(7)	161.97(8)	162.2(2)	161.3(3)	161.2(5)

cies were also varied, but in every case the refined values did not differ significantly from the stoichiometric composition [values ranging from 0.98(1) to 1.03(1), with 1.00 corresponding to full occupancy]. Therefore in all subsequent refinements the oxygen occupancy was fixed to 1.00. In the case of sample IIa (whose nuclear and magnetic structures are the same as those of the compound studied by Elemans *et al.*⁵), there is no doubt that the composition corresponds to stoichiometric LaMnO₃ within the limits of error of our measurements. It is more difficult to reach conclusions for samples IIb and III, which show the possible presence of cation vacancies. If we compare the results of refinements carried out assuming full occupancies for La and Mn with those obtained when these parameters were allowed to vary, we see that a lowering of the cation occupancies is invariably accompanied by a lowering of the temperature factors of these atoms, and by an increase of the temperature factors of the oxygen atoms. Similar results are also apparent in those

cases reported in the literature in which the authors have given not only the final R factors for the models tested, but also the atomic thermal parameters (e.g., compare models 1 and 2 in Table IV of Ref. 8). This behavior suggests that a loss of scattering power due to partial occupancy of the cation sites (and the consequent decrease in the cation/oxygen ratio) tends to be compensated by corresponding changes of the thermal factors. While our results indicate the presence of cationic vacancies, the correlation between occupancies and thermal factors makes it difficult to establish with certainty if the vacancies occur in equal number on the La and Mn sites. An answer to this question can only be inferred indirectly from other experiments, such as chemical analysis of Mn⁴⁺, detection of impurity lines from La₂O₃ or Mn₂O₃ in the powder patterns, etc. The results of Table II show that the R factors for the various models also vary only marginally. These refinements also showed that for the cases listed in Table II, the possible presence of low-concentration cation

vacancies does not introduce changes outside statistical uncertainties in the final values of the other structural parameters. For this reason the final results reported in this paper have been obtained assuming full occupancy for all atoms.

Examples of the agreement between observed and calculated intensities at 15 K are shown in Fig. 1(a) for the ferromagnetic (sample IIb) and Fig. 1(b) for the antiferromagnetic (sample IIa) orthorhombic phases, respectively. An excellent fit to the patterns is obtained, and, in particular, we find no evidence for any additional magnetic peaks that might result from a canted magnetic structure. There is also no evidence of any impurity phases in these data. Figure 2 shows the temperature dependence of the sublattice magnetization for the antiferromagnet, and the magnetization for the ferromagnets, for the various samples investigated. The ordered moments in the ground state are quite different for the different samples, but the ordering temperatures are comparable. Results of the final refinements of samples I, IIa, IIb, and III and relevant bond distances and angles, are given in Tables III–VI, respectively, for some of the temperatures considered. More complete lists of the results are available with the Physics Auxiliary Publication Service.¹²

The diffraction patterns of sample I (annealed in air) indicate the presence of two phases, one of which is orthorhombic (space group $Pnma$), while the other gives reflections that can be indexed equally well either in terms of a rhombohedral cell of symmetry $R\bar{3}c$, or in terms of a monoclinic, pseudorhombic cell of space group $P112_1/a$. Figure 3 shows a portion of the powder pattern illustrating the close relationship between the rhombohedral and monoclinic lattices and the resulting ambiguity in the indexing of the diffraction lines. The R factors obtained from the profile refinements, however, show that below 300 K the model $Pnma + P112_1/a$ gives better agreement between observed and calculated intensities than the model $Pnma + R\bar{3}c$. Above 300 K, the structural parameters of the monoclinic phase become highly correlated and the only refinable model is a mixture of the orthorhombic and rhombohedral phases (see Table III). In order to understand these results and to get an idea about the nature and the magnitude of the monoclinic distortion of the rhombohedral lattice, it is convenient to convert the rhombohedral cell into the corresponding pseudomonoclinic one by means of the transformation

$$(\vec{a}_M \vec{b}_M \vec{c}_M) = \left(\frac{2}{3}, \frac{1}{3}, -\frac{1}{3}/\frac{4}{3}, \frac{2}{3}, -\frac{1}{3}/0, 1, 0\right) \{\vec{a}_H \vec{b}_H \vec{c}_H\},$$

where \vec{a}_H , etc., and \vec{a}_M , etc., are the hexagonal and pseudomonoclinic axes, respectively, and the curly brackets indicate 3×1 matrices. In the absence of a distortion, this transformation yields the parameters of the pseudomonoclinic cell indicated by open circles in Fig. 4(a). Below 300 K, the refined parameters of the true monoclinic cell [indicated by solid circles in Fig. 4(a)] deviate smoothly from rhombohedral symmetry, and the magnitude of the deviation increases as the temperature decreases. This behavior makes it difficult to ascertain if the symmetry of the phase above 300 K is truly rhombohedral or if there is still a monoclinic distortion too small to be detected with the resolution of our experiment. The smooth variation with temperature of the lattice parameters of the monoclinic and orthorhombic phases [Figs. 4(a) and 4(b), respectively] indicates that there

TABLE IV. (Top) Structural parameters for LaMnO₃-IIa. Space group $Pnma$. (Bottom) Selected bond distances (Å) and angles (°) for LaMnO₃-IIa.

T (K)	14	121	300
a (Å)	5.7391(2)	5.7389(2)	5.7363(1)
b (Å)	7.6721(2)	7.6788(3)	7.6994(2)
c (Å)	5.5319(2)	5.5304(2)	5.5358(1)
V (Å ³)	243.58(2)	243.71(2)	244.50(1)
La x	-0.0482(3)	-0.0475(3)	-0.0475(3)
z	-0.0079(4)	-0.0081(3)	-0.0080(3)
B (Å ²)	0.32(3)	0.31(3)	0.62(3)
Mn B (Å ²)	0.37(6)	0.48(6)	0.51(6)
μ (μ_B)	3.65(3)	2.09(3)	
O(1) x	0.5144(4)	0.5137(4)	0.5131(4)
z	0.0753(4)	0.0749(4)	0.0752(4)
B (Å ²)	0.41(5)	0.43(4)	0.79(4)
O(2) x	0.1932(3)	0.1936(3)	0.1941(3)
y	0.0392(2)	0.0394(2)	0.0385(2)
z	-0.2252(3)	-0.2247(3)	-0.2256(3)
B (Å ²)	0.45(3)	0.42(3)	0.79(3)
R_p (%)	6.58	6.54	5.87
R_{wp} (%)	8.59	8.49	7.34
χ^2	1.559	1.434	1.285
La-O(1)	2.552(3)	2.560(3)	2.562(3)
La-O(1)	3.262(3)	3.254(3)	3.249(3)
La-O(1)	3.160(3)	3.155(3)	3.159(3)
La-O(1)	2.420(3)	2.421(3)	2.421(3)
La-O(2) $\times 2$	2.445(2)	2.443(2)	2.454(2)
La-O(2) $\times 2$	3.394(2)	3.394(2)	3.389(2)
La-O(2) $\times 2$	2.696(2)	2.701(2)	2.704(2)
La-O(2) $\times 2$	2.646(2)	2.647(2)	2.651(2)
Mn-O(1) $\times 2$	1.9646(5)	1.9655(5)	1.9708(4)
Mn-O(2) $\times 2$	2.178(2)	2.175(2)	2.174(2)
Mn-O(2) $\times 2$	1.906(2)	1.909(2)	1.907(2)
Mn-O(1)-Mn	155.0(1)	155.2(1)	155.2(1)
Mn-O(2)-Mn	154.84(9)	154.74(9)	155.4(8)

are no anomalies or detectable structural changes at the magnetic transition temperature (~ 130 K), in contrast to the situation found when the system is doped with Ca.¹⁰ Figure 4(c) shows how the relative amounts of the phases of sample I vary with temperature. Below ~ 100 K, when substantial magnetic intensities begin to appear at the positions of the nuclear reflections, the composition of the sample remains constant at 85 and 15 wt % of the orthorhombic and monoclinic phases, respectively. It is certainly possible that these two modifications have different ordering and/or magnitude of the magnetic moments. However, we have recently investigated the 33% Sr- and Ca-doped compounds¹³ which, in the ferromagnetic regime, have the same ordering of the magnetic moments, and nuclear structures of monoclinic and orthorhombic symmetry practically identical to those being investigated here. In view of these structural similarities it seems reasonable to assume that the two phases of sample I have the same magnetic structure. Magnetic reflections are absent (or very weak) when $h+k+l=2n+1$ and, for the class $h+k+l=2n$, when $k=2n+1$. This observation estab-

TABLE V. (Top) Structural parameters for LaMnO₃-IIB. (Bottom) Selected bond distances (Å) and angles (°) for LaMnO₃-IIB.

T (K)	300		
	15	300	
Space group	<i>Pnma</i>	<i>Pnma</i> (88 wt %)	$\bar{R}\bar{3}c$ (12 wt %)
<i>a</i> (Å)	5.4913(3)	5.4953(3)	5.5317(5)
<i>b</i> (Å)	7.7748(4)	7.7855(4)	
<i>c</i> (Å)	5.5268(3)	5.5355(3)	13.330(1)
<i>V</i> (Å ³)	235.96(3)	236.83(3)	353.25(6)
La <i>x</i>	-0.0233(3)	-0.0201(4)	
<i>z</i>	-0.0023(4)	-0.0028(5)	
<i>B</i> (Å ²)	0.58(3)	0.91(3)	0.91(3)
Mn <i>B</i> (Å ²)	0.38(4)	0.72(4)	0.72(4)
μ (μ _B)	2.94(4)		
O(1) <i>x</i>	0.5081(5)	0.5072(6)	0.443(1)
<i>z</i>	0.0666(5)	0.0633(5)	
<i>B</i> (Å ²)	0.87(5)	1.16(5)	1.06(5)
O(2) <i>x</i>	0.2260(3)	0.2279(4)	
<i>y</i>	0.0352(2)	0.0347(2)	
<i>z</i>	-0.2275(3)	-0.2286(4)	
<i>B</i> (Å ²)	0.62(3)	1.15(4)	
<i>R_p</i> (%)	6.73		6.30
<i>R_{wp}</i> (%)	8.58		7.89
χ^2	1.868		1.228
La-O(1)	2.601(3)	2.623(4)	2.450(8)×3
La-O(1)	2.943(3)	2.921(4)	3.082(8)×3
La-O(1)	3.123(4)	3.106(4)	2.7542(9)×6
La-O(1)	2.414(4)	2.438(4)	
La-O(2)×2	2.492(2)	2.496(3)	
La-O(2)×2	3.145(2)	3.130(2)	
La-O(2)×2	2.787(2)	2.803(2)	
La-O(2)×2	2.629(3)	2.634(3)	
Mn-O(1)×2	1.9787(5)	1.9781(5)	1.971(1)×6
Mn-O(2)×2	1.980(2)	1.978(2)	
Mn-O(2)×2	1.970(2)	1.974(2)	
Mn-O(1)-Mn	158.4(1)	159.5(2)	161.5(5)
Mn-O(2)-Mn	160.87(9)	161.4(1)	

lishes without ambiguity the ferromagnetic nature of the spin ordering. As in the doped compounds, the moments are aligned along the *c* axis, and the magnetic space groups are *Pn'm'a* and *P112₁/a* for the orthorhombic and monoclinic cases, respectively.

Sample II (annealed in N₂) is a mixture of two orthorhombic phases having the same nuclear space group symmetry *Pnma*, but considerably different lattice parameters (Table I). Below 100 K, these two modifications have different ordering of the magnetic moments. More specifically, one phase exhibits a ferromagnetic structure of the same type as that found in the orthorhombic compound of sample I. The other corresponds to a simple antiferromagnetic structure of space group *Pn'ma'* in which the spins are coupled ferromagnetically in the *a*, *c* planes and antiferromagnetically along the *b* axis [Fig. 7(e)]. Annealing in N₂ at 900 °C with a Ti getter transforms the mixture into the pure antiferromagnetic modification (sample IIa), while annealing in air at 1000 °C produces the ferromagnetic orthorhombic com-

pound, mixed, at room temperature, with small amounts of the rhombohedral phase $\bar{R}\bar{3}c$ (sample IIB). These results are consistent with published data. In fact, the room-temperature lattice parameters of phase IIa are in close agreement with those reported by Elemans *et al.* for LaMnO₃ (Ref. 5) and by Voorhoeve *et al.*¹⁴ for sample 1F (which contains only 2% of Mn⁴⁺). Phase $\bar{R}\bar{3}c$ of samples IIB and I, on the other hand, is the same as that reported by various workers⁶⁻⁸ (see also sample 2F of Ref. 14), for compositions LaMnO_{3+δ} with δ=0.13–0.15. Our results would also indicate that the orthorhombic ferromagnetic phase present in samples I, II, IIB, and III (which, to our knowledge, has not been reported previously) represents an intermediate stage between the oxidized phase $\bar{R}\bar{3}c$ of samples I and IIB, and the reduced antiferromagnetic phase *Pnma* of samples II and IIa. This conclusion is corroborated by the values of the average Mn-O distances which are, at 300 K, 1.971 Å in Mn⁴⁺-rich $\bar{R}\bar{3}c$, 1.977 Å in ferromagnetic *Pnma* [Table V (bottom)], and 2.017 Å in antiferromagnetic, stoichiometric *Pnma* [Table IV (bottom)]. Interestingly, the data of Table I seem to indicate that each of the two orthorhombic modifications exists over a range of values of the lattice parameters and, presumably, of compositions.

Figure 5 shows the variation of the lattice parameters of sample IIa with temperature. The overall volume decreases monotonically with decreasing temperature, but from room temperature to about 150 K the *a* axis shows negative thermal expansion, which becomes positive between 150 and 100 K, and negative again below 100 K. With decreasing temperature the *c* axis has positive thermal expansion down to 150 K and negative below this temperature, with a change of slope below 90 K. The *b* axis, on the other hand, decreases monotonically with temperature, with a small change of slope between 90 and 150 K. The length changes Δ*a/a* and Δ*c/c* are about 0.1% and, with the resolution of our experiment, we have not been able to correlate these changes with corresponding effects in the nuclear and/or magnetic structure. A somewhat similar behavior of the lattice parameters has been found by Argyriou *et al.*¹⁵ in the canted ferromagnetic insulator La_{0.875}Sr_{0.125}MnO_{3+δ}. This compound is also orthorhombic and the length changes are of the order of 0.4%. The authors were able to correlate the variation of lattice parameters with corresponding variations of the Mn-O bond lengths resulting in a large breathing motion of the MnO₆ octahedra. A similar situation is possible also in our case, but with length changes much smaller than those found in the Sr-doped compound.

IV. DISCUSSION

The relationship between the lattice parameters of the phases described in this paper and those of perovskite is illustrated in Fig. 6. The rhombohedral structure can be derived from the undistorted configuration of perovskite by tilting the MnO₆ octahedra about each of the three fourfold axes of the cubic cell by the same angle (about 9° in our case) but with opposite sense of rotation for consecutive octahedra. This tilt system has been indicated with the symbol *a⁻a⁻a⁻* (Ref. 16) and is equivalent to a rotation about one of the original three-fold axes of the cubic cell.¹⁷ The result-

TABLE VI. Structural parameters and selected bond distances (\AA) and angles (deg) for $\text{LaMnO}_3\text{-III}$. Space group $Pnma$.

T (K)	Structural parameters		Bond distances and angles			
	10	300	10	300		
	a (\AA)	5.4948(2)	5.4975(2)	La-O(1)	2.598(3)	2.617(3)
	b (\AA)	7.7749(3)	7.7867(3)	La-O(1)	2.952(3)	2.932(3)
	c (\AA)	5.5252(2)	5.5341(2)	La-O(1)	3.112(3)	3.104(3)
	V (\AA^3)	236.04(2)	236.90(3)	La-O(1)	2.425(3)	2.440(3)
				La-O(2) \times 2	2.481(2)	2.487(2)
La	x	-0.0249(3)	-0.0218(3)	La-O(2) \times 2	3.166(2)	3.149(2)
	z	-0.0040(4)	-0.0037(4)	La-O(2) \times 2	2.784(2)	2.800(2)
	B (\AA^2)	0.57(3)	0.83(3)	La-O(2) \times 2	2.627(2)	2.632(2)
Mn	B (\AA^2)	0.30(4)	0.57(4)	Mn-O(1) \times 2	1.9784(4)	1.9788(4)
	μ (μ_B)	2.68(5)		Mn-O(2) \times 2	1.980(2)	1.977(2)
				Mn-O(2) \times 2	1.975(2)	1.979(2)
O(1)	x	0.5077(4)	0.5071(5)			
	z	0.0663(4)	0.0638(4)	Mn-O(1)-Mn	158.5(1)	159.3(1)
	B (\AA^2)	0.72(7)	1.34(8)	Mn-O(2)-Mn	160.26(8)	160.81(8)
O(2)	x	0.2246(3)	0.2268(3)			
	y	0.0358(2)	0.0354(3)			
	z	-0.2256(3)	-0.2269(3)			
	B (\AA^2)	0.71(5)	1.15(5)			
	R_p (%)	6.14	5.38			
	R_{wp} (%)	7.94	6.85			
	χ^2	1.681	1.439			

ing configuration of the octahedra in consecutive layers is illustrated in Fig. 7. The O-Mn-O bond angles are given in Fig. 8 and they show that, in addition to the tilting, the octahedra of the rhombohedral phase are also slightly distorted.

The Mn-O distances and O-Mn-O angles in the two non-equivalent MnO_6 octahedra of the $P112_1/a$ structure are not significantly different from each other and are remarkably similar to those found in the $R\bar{3}c$ structure. This result shows that the distortion of the octahedra is essentially the same in the rhombohedral and monoclinic phases and that the cations Mn^{3+} and Mn^{4+} are randomly distributed in the monoclinic structure. Qualitatively, the tilt of the MnO_6 octahedra is also similar in $P112_1/a$ and $R\bar{3}c$. Due to the high values of the

standard deviations on the tilt angles, however, it is difficult to establish with certainty if the tilt system is identical in the two cases. As shown in Table III (top), the La cations of the monoclinic structure are slightly shifted from the special positions they occupy in the rhombohedral cell, and this shift may well be accompanied by a small departure of the tilt system from the $a^-a^-a^-$ configuration. The displacement of La occurs roughly along one of the cell diagonals and is antiparallel in successive layers along the direction of the b axis.

The structures of both orthorhombic phases are generated from that of undistorted perovskite by tilting the MnO_6 octahedra according to the tilt system $a^+b^-b^-$.¹⁶ The magni-

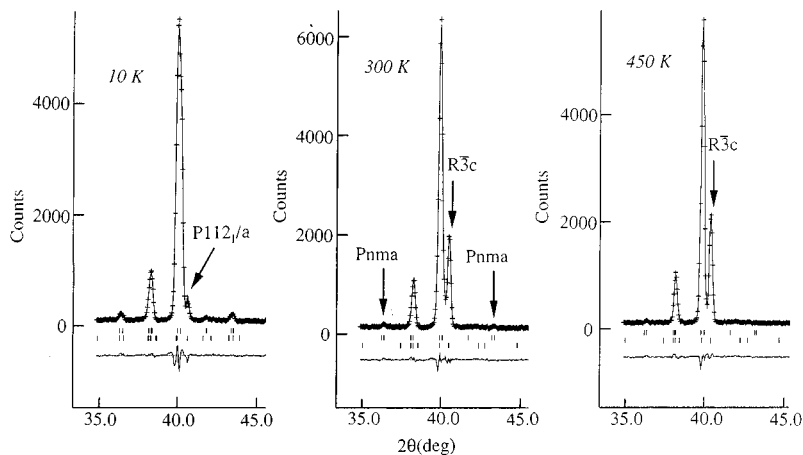


FIG. 3. Part of the powder pattern from sample I. The short vertical lines indicate the angular positions of Bragg reflections generated by the orthorhombic phase (top rows) and by the monoclinic (at 10 K) and rhombohedral phases (bottom rows).

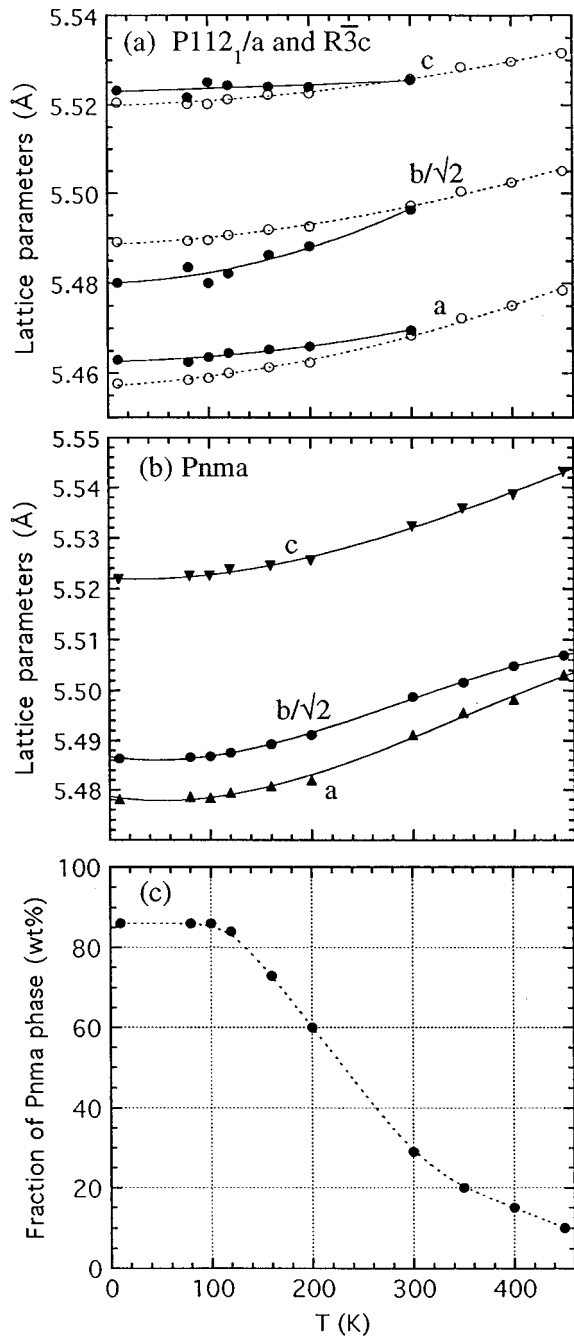


FIG. 4. Variation with temperature of the lattice parameters and composition of the phases present in sample I. In (a) the full circles represent the parameters of $P112_1/a$ and the open circles those of $R\bar{3}c$.

tude of the tilt angle is different in the two cases, however, being 9° – 10° (i.e., similar to that of the $R\bar{3}c$ and $P112_1/a$ phases) and 12° – 13° for the ferro- and the antiferromagnetic modifications, respectively. The atomic configuration produced by the system $a^+b^-b^-$ is basically different from that of the monoclinic and rhombohedral phases, since in this case the sense of tilting along one of the crystallographic axes (the b axis, with our choice of the reference system) is the same, rather than opposite, for consecutive octahedra. In the orthorhombic ferromagnetic modification, the MnO_6 oc-

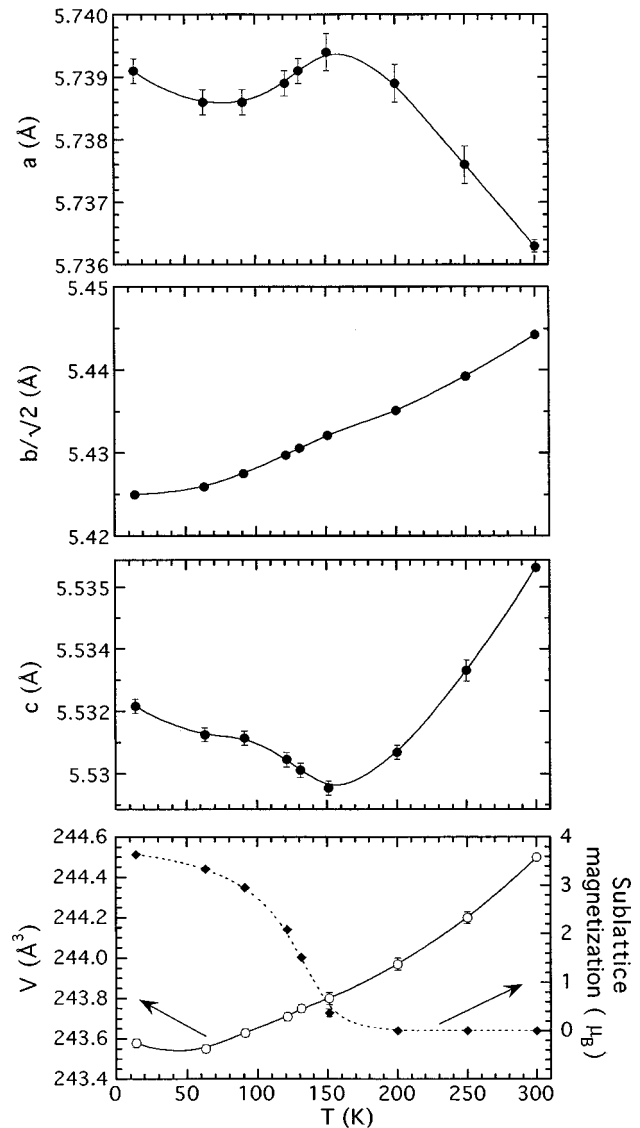


FIG. 5. Variation with temperature of the lattice parameters, unit-cell volume, and sublattice magnetization obtained from the refinements of the antiferromagnetic orthorhombic phase of sample IIa.

tahedra are only slightly distorted (in a manner similar to that discussed for the rhombohedral and monoclinic phases), with Mn-O distances nearly equal (1.98, 1.97, and 1.98 \AA at 300 K) and with O-Mn-O angles differing from 90° by less than 2° . In the case of the antiferromagnetic structure, however, the Mn-O distances become 1.97, 2.17, and 1.91 \AA at 300 K (with the O-Mn-O angles $\sim 90.3^\circ$), thus showing a much more pronounced distortion of the octahedra. These bond distances and angles are in very good agreement with the values reported for $LaMnO_3$ in Table II of Ref. 5. Also the shifts of the La cations are more pronounced in the antiferromagnetic than in the ferromagnetic structure, resulting in LaO_{12} cages in which the La-O distances range from 2.42 to 3.39 \AA in the first case and from 2.48 to 3.14 \AA in the second.

As we have mentioned previously, our results have confirmed the existence of cationic vacancies but we were unable to determine their ratio. Other results, however, support

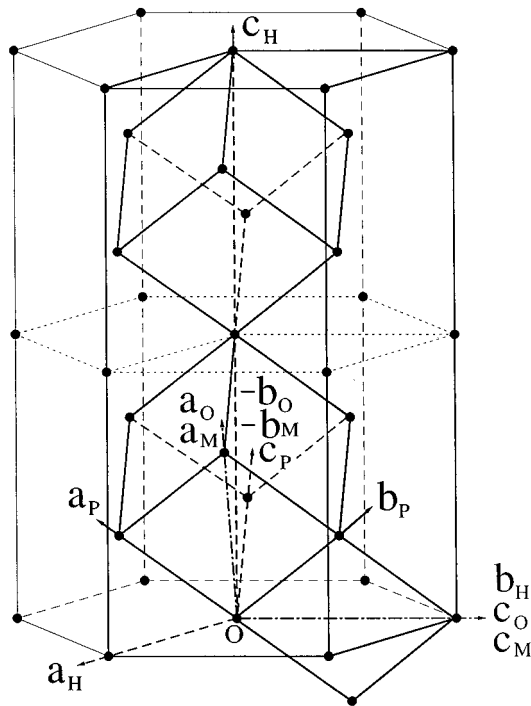
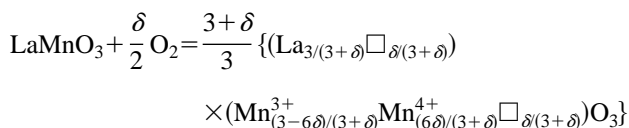


FIG. 6. Relationship between the crystallographic axes of perovskite and those of phases $R\bar{3}c$, $P112_1/a$, and $Pnma$. The transformation matrices needed to obtain the unit cells of these phases from the unit cell of perovskite are (i) $(1\ 0\ -1\ /\ -1\ 1\ 0\ /\ 2\ 2\ 2)$ for $R\bar{3}c$ (hexagonal axes); (ii) $(1\ 1\ 0\ /\ 0\ 1\ 1\ /\ 1\ 0\ 1)$ for $R\bar{3}c$ (rhombohedral axes); (iii) $(1\ 1\ 0\ /\ 0\ 0\ -2\ /\ -1\ 1\ 0)$ for $P112_1/a$ and $Pnma$.

their occurrence in equal number on the La and Mn sites of the structure. These include (i) the presence of about 30% of Mn^{4+} in the $R\bar{3}c$ phase (and of only 2% in the $Pnma$ antiferromagnetic phase);¹⁴ (ii) the lack of evidence for interstitial oxygen or oxygen vacancies; (iii) the absence of extra phases in high-resolution transmission electron microscopy studies,⁷ or impurity lines of La_2O_3 and/or Mn_2O_3 in x-ray and neutron powder diffraction patterns (Refs. 6, 7, present work); (iv) thermogravimetric¹⁸ and density analyses.¹⁹ The oxireduction process in the undoped lanthanum manganite can therefore be represented with the following chemical reaction proposed by Roosmalen and Cordfunke:¹⁸



which implies equal number of La and Mn vacancies and a stoichiometric oxygen sublattice.

The structural features and the magnetic ordering of the various phases described previously are in general agreement with the predictions derived by Goodenough from the character of the manganese-oxygen bonding.⁴ In the case of the orthorhombic structure of sample IIa, the Mn^{3+} ions are ordered ferromagnetically in the a, c plane below the Curie temperature and have Mn-O bond distances of 2.178 and 1.906 Å. These separations correspond to ionic and semico-

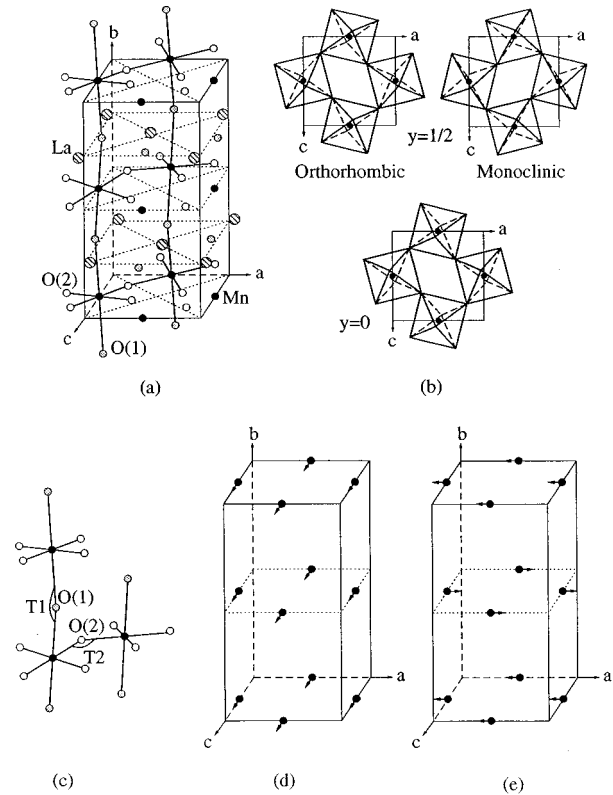


FIG. 7. Schematic representation of the nuclear and magnetic structures in the lanthanum manganite system: (a) nuclear structure represented in the $Pnma$ reference system; (b) tilting of the MnO_6 octahedra in two successive layers along b ; (c) tilt angles of the octahedra; (d) ferromagnetic structure of phases $P112_1/a$ and $Pnma$; (e) antiferromagnetic structure of phase $Pnma$ (sample IIa).

valent bonding, respectively, and the spin coupling in the plane is consistent with case 2 in Table I of Ref. 4. Along the b axis, on the other hand, both Mn^{3+} ions are bonded semicovalently to the two neighboring oxygen ions, with Mn-O distance of 1.965 Å, and are coupled antiferromagnetically, as predicted by case 1. If the orthorhombic lattice parameters at 10 K are transformed into those of the perovskite cell a_p, b_p, c_p by means of the transformation matrix $(\frac{1}{2}\ 0\ \frac{1}{2}/\ \frac{1}{2}\ 0/\ -\frac{1}{2}\ 0\ \frac{1}{2})$, we obtain $b_p/c_p = 0.967$ and $\Delta \equiv (c_p - b_p)/c_p = 0.037$. These values are in good agreement with those predicted by Goodenough (0.959 and 0.041, respectively) for the composition $x=0$, x being the fraction of Mn^{4+} ions in the structure. For the antiferromagnetic phase of sample II, it is $b_p/c_p = 0.971$ and $\Delta = 0.029$. Again, these values are consistent with Goodenough's predictions for the composition range $0 < x < 0.1$ and indicate a slight change in the distribution of the Mn-O bonding in the a, c plane due to the presence of a small number of Mn^{4+} ions.

If the concentration of the Mn^{4+} ions is sufficiently high ($x \approx 0.25$) and if Mn^{3+} and Mn^{4+} are randomly distributed, cases 1 and 2, which dominate the bonding type in the antiferromagnetic structure, cannot exist anymore and are replaced by the metalliclike bond represented by case 4 in Ref. 4. This means that, below the Curie temperature, ferromagnetic double exchange between the Mn ions takes place

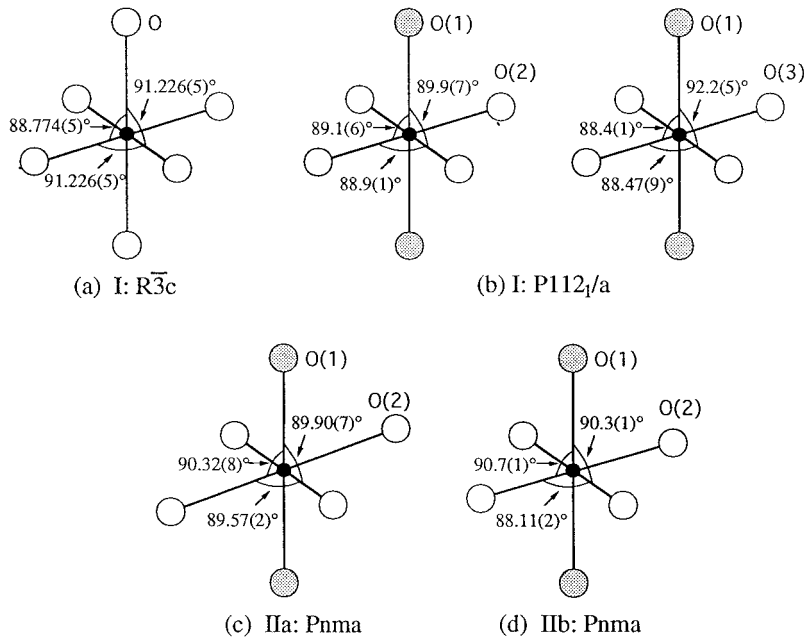


FIG. 8. O-Mn-O angles in the MnO_6 octahedra for the phases of the system. The Roman numerals before the space group symbols indicate the sample in which the phase was found.

along all three crystallographic directions. This new configuration will result in a significant reduction in the distortion of the MnO_6 octahedra. These theoretical predictions are confirmed by the magnetic properties and the general structural features of the orthorhombic phase present in samples IIb and III, which is ferromagnetic below ~ 140 K and in which the three Mn-O separations are approximately equal. The ratios b_p/c_p of the ferromagnetic structure present in samples II and III (0.980 and 0.998, respectively) also show that this phase exists in a range of compositions, as shown by the phase diagram of Fig. 5 in Ref. 4.

The symmetry of the ferromagnetic phase predicted by Goodenough, however, is rhombohedral rather than orthorhombic. We have observed an orthorhombic to rhombohedral transition in samples I and IIb (see Table I), but with the rhombohedral phase appearing at room temperature. A thermally induced structural change of the same type has also been observed in the system $La_{1-x}Sr_xMnO_3$ in the range of composition $0.15 < x < 0.20$ and has been attributed to changes in the ionic sizes of the constituent ions.²⁰ As we have mentioned previously, the structures of the orthorhombic and rhombohedral phases are significantly different since they are characterized by different tilt systems of the MnO_6 octahedra. It is therefore interesting that both in the undoped and in the Sr-doped systems the basic ordering of the magnetic spins remains unaffected by such a large rearrangement of the nuclear structure.

As shown in Table I, sample II is a mixture of the ferro- and antiferromagnetic orthorhombic phases. This result is not surprising because this sample was prepared by incomplete reduction of sample I and, according to Goodenough's phase diagram, a mixture of two phases is predicted in the composition range $0.1 < x < 0.25$. A portion of the diagram is reproduced in Fig. 9, where the unit-cell volume found in this study for the ferro- and antiferromagnetic orthorhombic structures is plotted against the compositions predicted by Goodenough. Here the volume is determined from the diffraction results, while the concentration of Mn^{4+} is determined by assuming that sample IIa is fully reduced and

sample IIb is fully oxygenated orthorhombic. Sample II is a mixed phase, and thus must lie on either side of the mixed-phase region $\alpha + \beta$. These assumed concentrations for Mn^{4+} are consistent with our determined defect concentration on the Mn and La sites, and we see that the experimentally determined volumes then lie on a straight line.

In summary, using neutron crystallographic techniques we have reconciled the apparent discrepancies among the reported magnetic structures for undoped $LaMnO_3$ prepared by different procedures. Our analysis indicates that the stoichiometric compound is orthorhombic of space group $Pnma$, and that the moments order antiferromagnetically along the b -axis direction. With the gradual introduction of cation vacancies on the La and Mn sites by annealing in an oxygen-rich atmosphere, the crystalline structure changes first from orthorhombic antiferromagnetic to orthorhombic ferromagnetic, $Pnma$. This intermediate orthorhombic

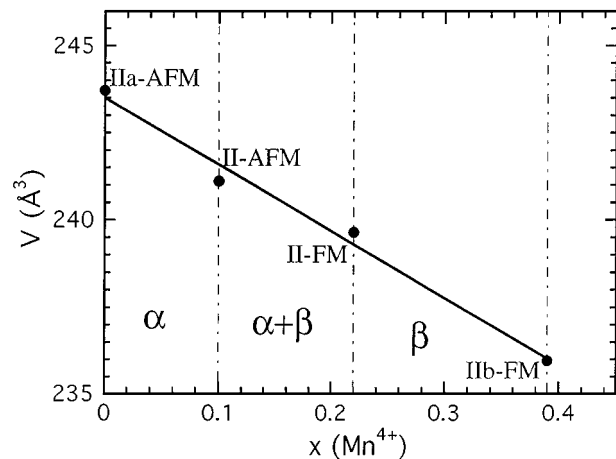


FIG. 9. Plot of the unit-cell volumes of the orthorhombic phases in samples II, IIa, and IIb vs the compositions predicted by Goodenough (Ref. 4).

phase, which has not been observed previously, has a substantially smaller unit-cell volume in comparison to the stoichiometric compound. Further oxygenation then leads to a monoclinic phase, space group $P112_1/a$, which is also ferromagnetic below ~ 130 K. With increasing temperature the monoclinic distortion becomes smaller, and above room temperature it is not possible to distinguish this from a rhombohedral phase of space group $R\bar{3}c$. The magnetic ordering temperature, on the other hand, is not particularly sensitive to these structural changes even though the magnetic structure changes from antiferromagnetic to ferromagnetic. We find that the antiferromagnetic orthorhombic phase can easily be recovered and the preparation processes are fully reversible. Our observed phases and their corresponding magnetic struc-

tures agree well with the theoretical predictions of Goodenough regarding the dependence on the Mn-O bonding and the Mn-Mn magnetic exchange. These results provide a firm basis for understanding the evolution of the structural and magnetic properties of doped LaMnO_3 compounds, which we will discuss in a future paper.

ACKNOWLEDGMENTS

We would like to thank S. M. Bhagat, R. S. Roth, and T. A. Vanderah for helpful discussions. Research at the University of Maryland was supported in part by the NSF, DMR 93-02380.

-
- ¹S. Jin, T. H. Tiefel, M. McCormack, R. A. Fastnacht, R. Ramesh, and L. H. Chen, *Science* **264**, 413 (1994); S. Jin, M. McCormack, T. H. Tiefel, and R. Ramesh, *J. Appl. Phys.* **76**, 6929 (1994).
- ²E. O. Wollan and W. C. Koehler, *Phys. Rev.* **100**, 545 (1955).
- ³H. L. Yakel, Jr., *Acta. Crystallogr.* **8**, 394 (1955).
- ⁴J. B. Goodenough, *Phys. Rev.* **100**, 564 (1955).
- ⁵J. B. A. A. Elemans, B. Van Laar, K. R. Van Der Veen, and B. O. Loopstra, *J. Solid State Chem.* **3**, 238 (1971).
- ⁶B. C. Tofield and W. R. Scott, *J. Solid State Chem.* **10**, 183 (1974).
- ⁷J. A. M. van Roosmalen, E. H. P. Cordfunke, R. B. Helmholdt, and H. W. Zandbergen, *J. Solid State Chem.* **110**, 100 (1994).
- ⁸V. Ferris, L. Brohan, M. Ganne, and M. Tournoux, *Eur. J. Solid State Inorg. Chem.* **32**, 131 (1995).
- ⁹P. Schiffer, A. P. Ramirez, W. Bao, and S-W. Cheong, *Phys. Rev. Lett.* **75**, 3336 (1995).
- ¹⁰J. W. Lynn, R. W. Erwin, J. A. Borchers, Q. Huang, A. Santoro, J-L. Peng, and Z. Y. Li, *Phys. Rev. Lett.* **76**, 4046 (1996).
- ¹¹A. C. Larson and R. B. Von Dreele, *General Structure Analysis System*, Report No. LAUR-86-748, Los Alamos National Laboratory, Los Alamos, NM 87545 (1990).
- ¹²See AIP Document No. E-PAPS: E-PRBMDO-55-14987 for lists of results. E-PAPS document files may be retrieved free of charge from our FTP server (<http://www.aip.org/epaps/epaps.html>) or from <ftp.aip.org> in the directory /epaps/. For further information: e-mail: PAPS@aip.org or fax: 516-576-2223.
- ¹³Q. Huang *et al.* (private communication).
- ¹⁴R. J. H. Voorhoeve, J. P. Remeika, L. E. Trimble, A. S. Cooper, F. J. DiSalvo, and P. K. Gallagher, *J. Solid State Chem.* **14**, 395 (1975).
- ¹⁵D. N. Argyriou, J. F. Mitchell, C. D. Potter, D. G. Hinks, J. D. Jorgensen, and S. D. Bader, *Phys. Rev. Lett.* **76**, 3826 (1996).
- ¹⁶A. M. Glazer, *Acta. Crystallogr. B* **28**, 3384 (1972); **A** **31**, 756 (1975).
- ¹⁷M. O'Keeffe and B. G. Hyde, *Acta. Crystallogr. B* **33**, 3802 (1977).
- ¹⁸J. A. M. van Roosmalen and E. H. P. Cordfunke, *J. Solid State Chem.* **110**, 109 (1994).
- ¹⁹J. A. M. van Roosmalen and E. H. P. Cordfunke, *J. Solid State Chem.* **110**, 106 (1994).
- ²⁰A. Asamitsu, Y. Moritomo, Y. Tomioka, T. Arima, and Y. Tokura, *Nature* **373**, 407 (1995).